DESY 93-137 ISSN 0418-9833
October 1993

A Measurement of Multi-jet Rates in Deep-Inelastic Scattering at HERA

H1 Collaboration

Abstract:

Multi-jet production is observed in deep-inelastic electron proton scattering with the H1 detector at HERA. Jet rates for momentum transfers squared up to 500 GeV^2 are determined using the JADE jet clustering algorithm. They are found to be in agreement with predictions from QCD based models.

H1 Collaboration

I. Abt[7], T. Ahmed[3], V. Andreev[24], B. Andrieu[27], R.-D. Appuhn[11], M. Arpagaus[34],
A. Babaev[25], H. Bärwolff[33], J. Bán[17], P. Baranov[24], E. Barrelet[28], W. Bartel[11], U. Bassler[28],
H.P. Beck[35], H.-J. Behrend[11], A. Belousov[24], Ch. Berger[1], H. Bergstein[1], G. Bernardi[28],
R. Bernet[34], G. Bertrand-Coremans[4], M. Besançon[9], P. Biddulph[22], E. Binder[11], A. Bischoff[33],
J.C. Bizot[26], V. Blobel[13], K. Borras[8], P.C. Bosetti[2], V. Boudry[27], C. Bourdarios[26], F. Brasse[11],
U. Braun[2], W. Braunschweig[1], V. Brisson[26], D. Bruncko[17], L. Büngener[13], J. Bürger[11],
F.W. Büsser[13], A. Buniatian[11,37], S. Burke[19], G. Buschhorn[25], A.J. Campbell[1], T. Carli[25],
F. Charles[28], D. Clarke[5], A.B. Clegg[18], M. Colombo[8], J.A. Coughlan[5], A. Courau[26],
Ch. Coutures[9], G. Cozzika[9], L. Criegee[11], J. Cvach[27], S. Dagoret[28], J.B. Dainton[19],
M. Danilov[23], A.W.E. Dann[22], W.D. Dau[16], M. David[9], E. Deffur[11], B. Delcourt[26],
L. Del Buono[28], M. Devel[26], A. De Roeck[11], P. Dingus[27], C. Dollfus[35], J.D. Dowell[3],
H.B. Dreis[2], A. Drescher[8], J. Duboc[28], D. Düllmann[13], O. Dünger[13], H. Duhm[12],
R. Ebbinghaus[8], M. Eberle[12], J. Ebert[32], T.R. Ebert[19], G. Eckerlin[11], V. Efremenko[23],
S. Egli[35], S. Eichenberger[35], R. Eichler[34], F. Eisele[14], E. Eisenhandler[20], N.N. Ellis[3],
R.J. Ellison[22], E. Elsen[11], M. Erdmann[14], E. Evrard[4], L. Favart[4], A. Fedotov[23], D. Feeken[13],
R. Felst[11], J. Feltesse[9], I.F. Fensome[3], J. Ferencei[11], F. Ferrarotto[31], K. Flamm[11],
W. Flauger[11,†], M. Fleischer[11], M. Flieser[25], G. Flügge[2], A. Fomenko[24], B. Fominykh[23],
M. Forbush[7], J. Formánek[30], J.M. Foster[22], G. Franke[11], E. Fretwurst[12], P. Fuhrmann[1],
E. Gabathuler[19], K. Gamerdinger[25], J. Garvey[3], J. Gayler[11], A. Gellrich[13], M. Gennis[11],
H. Genzel[1], R. Gerhards[11], L. Godfrey[7], U. Goerlach[11], L. Goerlich[6], M. Goldberg[28],
A.M. Goodall[19], I. Gorelov[23], P. Goritchev[23], C. Grab[34], H. Grässler[2], R. Grässler[2],
T. Greenshaw[19], H. Greif[25], G. Grindhammer[25], C. Gruber[16], J. Haack[33], D. Haidt[11],
L. Hajduk[6], O. Hamon[28], D. Handschuh[11], E.M. Hanlon[18], M. Hapke[11], J. Harjes[11],
R. Haydar[26], W.J. Haynes[5], J. Heatherington[20], V. Hedberg[21], G. Heinzelmann[13],
R.C.W. Henderson[18], H. Henschel[33], R. Herma[1], I. Herynek[29], W. Hildesheim[11], P. Hill[11],
C.D. Hilton[22], J. Hladký[29], K.C. Hoeger[22], Ph. Huet[4], H. Hufnagel[14], N. Huot[28],
M. Ibbotson[22], H. Itterbeck[1], M.-A. Jabiol[9], A. Jacholkowska[26], C. Jacobsson[21], M. Jaffre[26],
T. Jansen[11], L. Jönsson[21], K. Johannsen[13], D.P. Johnson[4], L. Johnson[18], H. Jung[2],
P.I.P. Kalmus[20], S. Kasarian[11], R. Kaschowitz[2], P. Kasselmann[12], U. Kathage[16],
H. H.Kaufmann[33], I.R. Kenyon[3], S. Kermiche[26], C. Keuker[1], C. Kiesling[25], M. Klein[33],
C. Kleinwort[13], G. Knies[11], W. Ko[7], T. Köhler[1], H. Kolanoski[8], F. Kole[7], S.D. Kolya[22],
V. Korbel[11], M. Korn[8], P. Kostka[33], S.K. Kotelnikov[24], M.W. Krasny[6,28], H. Krehbiel[11],
D. Krücker[2], U. Krüger[11], J.P. Kubenka[25], H. Küster[2], M. Kuhlen[25], T. Kurča[17],
J. Kurzhöfer[8], B. Kuznik[32], D. Lacour[28], F. Lamarche[27], R. Lander[7], M.P.J. Landon[20],
W. Lange[33], R. Langkau[12], P. Lanius[25], J.F. Laporte[9], A. Lebedev[24], A. Leuschner[11],
C. Leverenz[11], S. Levonian[11,24], D. Lewin[11], Ch. Ley[2], A. Lindner[8], G. Lindström[12],
F. Linsel[11], J. Lipinski[13], P. Loch[11], H. Lohmander[21], G.C. Lopez[20], D. Lüers[25,†],
N. Magnussen[32], E. Malinovski[24], S. Mani[7], P. Marage[4], J. Marks[10], R. Marshall[22],
J. Martens[32], R. Martin[19], H.-U. Martyn[1], J. Martyniak[6], S. Masson[2], A. Mavroidis[20],
S.J. Maxfield[19], S.J. McMahon[19], A. Mehta[22], K. Meier[15], D. Mercer[22], T. Merz[11],
C.A. Meyer[35], H. Meyer[32], J. Meyer[11], S. Mikocki[6,26], V. Milone[31], E. Monnier[28], F. Moreau[27],
J. Moreels[4], J.V. Morris[5], K. Müller[35], P. Murín[17], S.A. Murray[22], V. Nagovizin[23],

B. Naroska[13], Th. Naumann[33], P.R. Newman[3], D. Newton[18], D. Neyret[28], H.K. Nguyen[28], F. Niebergall[13], C. Niebuhr[11], R. Nisius[1], G. Nowak[6], G.W. Noyes[3], M. Nyberg[21], H. Oberlack[25], U. Obrock[8], J.E. Olsson[11], S. Orenstein[27], F. Ould-Saada[13], C. Pascaud[26], G.D. Patel[19], E. Peppel[11], S. Peters[25], H.T. Phillips[3], J.P. Phillips[22], Ch. Pichler[12], W. Pilgram[2], D. Pitzl[34], S. Prell[11], R. Prosi[11], G. Rädel[11], F. Raupach[1], K. Rauschnabel[8], P. Reimer[29], S. Reinshagen[11], P. Ribarics[25], V. Riech[12], J. Riedlberger[34], S. Riess[13], M. Rietz[2], S.M. Robertson[3], P. Robmann[35], R. Roosen[4], A. Rostovtsev[23], C. Royon[9], M. Rudowicz[25], M. Ruffer[12], S. Rusakov[24], K. Rybicki[6], N. Sahlmann[2], E. Sanchez[25], D.P.C. Sankey[5], M. Savitsky[11], P. Schacht[25], P. Schleper[14], W. von Schlippe[20], C. Schmidt[11], D. Schmidt[32], W. Schmitz[2], A. Schöning[11], V. Schröder[11], M. Schulz[11], B. Schwab[14], A. Schwind[33], W. Scobel[12], U. Seehausen[13], R. Sell[11], A. Semenov[23], V. Shekelyan[23], I. Sheviakov[24], H. Shooshtari[25], L.N. Shtarkov[24], G. Siegmon[16], U. Siewert[16], Y. Sirois[27], I.O. Skillicorn[10], P. Smirnov[24], J.R. Smith[7], L. Smolik[11], Y. Soloviev[24], H. Spitzer[13], P. Staroba[29], M. Steenbock[13], P. Steffen[11], R. Steinberg[2], B. Stella[31], K. Stephens[22], J. Stier[11], U. Stösslein[33], J. Strachota[11], U. Straumann[35], W. Struczinski[2], J.P. Sutton[3], R.E. Taylor[36,26], V. Tchernyshov[23], C. Thiebaux[27], G. Thompson[20], I. Tichomirov[23], P. Truöl[35], J. Turnau[6], J. Tutas[14], L. Urban[25], A. Usik[24], S. Valkar[30], A. Valkarova[30], C. Vallée[28], P. Van Esch[4], A. Vartapetian[11,37], Y. Vazdik[24], M. Vecko[29], P. Verrecchia[9], R. Vick[13], G. Villet[9], E. Vogel[1], K. Wacker[8], I.W. Walker[18], A. Walther[8], G. Weber[13], D. Wegener[8], A. Wegner[11], H. P.Wellisch[25], L.R. West[3] S. Willard[7], M. Winde[33], G.-G. Winter[11], Th. Wolff[34], L.A. Womersley[19], A.E. Wright[22], N. Wulff[11], T.P. Yiou[28], J. Žáček[30], P. Závada[29], C. Zeitnitz[12], H. Ziaeepour[26], M. Zimmer[11], W. Zimmermann[11] and F. Zomer[26]

[1] *I. Physikalisches Institut der RWTH, Aachen, Germany*[a]
[2] *III. Physikalisches Institut der RWTH, Aachen, Germany*[a]
[3] *School of Physics and Space Research, University of Birmingham, Birmingham, UK*[b]
[4] *Inter-University Institute for High Energies ULB-VUB, Brussels, Belgium*[c]
[5] *Rutherford Appleton Laboratory, Chilton, Didcot, UK*[b]
[6] *Institute for Nuclear Physics, Cracow, Poland*[d]
[7] *Physics Department and IIRPA, University of California, Davis, California, USA*[e]
[8] *Institut für Physik, Universität Dortmund, Dortmund, Germany*[a]
[9] *DAPNIA, Centre d'Etudes de Saclay, Gif-sur-Yvette, France*
[10] *Department of Physics and Astronomy, University of Glasgow, Glasgow, UK*[b]
[11] *DESY, Hamburg, Germany*[a]
[12] *I. Institut für Experimentalphysik, Universität Hamburg, Hamburg, Germany*[a]
[13] *II. Institut für Experimentalphysik, Universität Hamburg, Hamburg, Germany*[a]
[14] *Physikalisches Institut, Universität Heidelberg, Heidelberg, Germany*[a]
[15] *Institut für Hochenergiephysik, Universität Heidelberg, Heidelberg, Germany*[a]
[16] *Institut für Reine und Angewandte Kernphysik, Universität Kiel, Kiel, Germany*[a]
[17] *Institute of Experimental Physics, Slovak Academy of Sciences, Košice, Slovak Republik*
[18] *School of Physics and Materials, University of Lancaster, Lancaster, UK*[b]
[19] *Department of Physics, University of Liverpool, Liverpool, UK*[b]
[20] *Queen Mary and Westfield College, London, UK*[b]
[21] *Physics Department, University of Lund, Lund, Sweden*[f]

[22] *Physics Department, University of Manchester, Manchester, UK*[b]
[23] *Institute for Theoretical and Experimental Physics, Moscow, Russia*
[24] *Lebedev Physical Institute, Moscow, Russia*
[25] *Max-Planck-Institut für Physik, München, Germany*[a]
[26] *LAL, Université de Paris-Sud, IN2P3-CNRS, Orsay, France*
[27] *LPNHE, Ecole Polytechnique, IN2P3-CNRS, Palaiseau, France*
[28] *LPNHE, Universités Paris VI and VII, IN2P3-CNRS, Paris, France*
[29] *Institute of Physics, Czech Academy of Sciences, Praha, Czech Republik*
[30] *Nuclear Center, Charles University, Praha, Czech Republik*
[31] *INFN Roma and Dipartimento di Fisica, Universita "La Sapienzia", Roma, Italy*
[32] *Fachbereich Physik, Bergische Universität Gesamthochschule Wuppertal, Wuppertal, Germany*[a]
[33] *DESY, Institut für Hochenergiephysik, Zeuthen, Germany*[a]
[34] *Institut für Mittelenergiephysik, ETH, Zürich, Switzerland*[g]
[35] *Physik-Institut der Universität Zürich, Zürich, Switzerland*[g]
[36] *Stanford Linear Accelerator Center, Stanford California, USA*
[37] *Visitor from Yerevan Phys.Inst., Armenia*
† *Deceased*

[a] *Supported by the Bundesministerium für Forschung und Technologie, FRG under contract numbers 6AC17P, 6AC47P, 6DO57I, 6HH17P, 6HH27I, 6HD17I, 6HD27I, 6KI17P, 6MP17I, and 6WT87P*
[b] *Supported by the UK Science and Engineering Research Council*
[c] *Supported by IISN-IIKW, NATO CRG-890478*
[d] *Supported by the Polish State Committee for Scientific Research, grant No. 204209101*
[e] *Supported in part by USDOE grant DE F603 91ER40674*
[f] *Supported by the Swedish Natural Science Research Council*
[g] *Supported by the Swiss National Science Foundation*

1 Introduction

The study of deep-inelastic lepton scattering (DIS) off protons has been extensively used for quantitative tests of QCD. To date most experiments have studied the evolution of the inclusive structure functions with momentum transfer Q^2, which is predicted in perturbative QCD. First measurements of QCD effects in the hadronic final states have been performed by fixed target experiments[1] and jet analyses have been carried out [2]. These measurements suffer, however, from the limited available energy and therefore limited phase space in which to observe multi-jet production. This situation has changed with the advent of the HERA electron-proton collider. With 26.7 GeV electrons incident on 820 GeV protons, the accessible range in Q^2 is about two orders of magnitude larger than in fixed target experiments. With our 1992 data sample and an integrated luminosity of 22.5 nb^{-1}, we give results on jet rates for values of Q^2 up to 500 GeV^2, including events with Q^2 up to 2600 GeV^2. The invariant mass W of the final state hadrons ranges from about 70 to 230 GeV, in contrast with e^+e^- experiments which typically measure at fixed W.

DIS from a proton constituent produces one or more partons with large transverse momentum (p_t), which manifest themselves as high p_t jets plus a proton remnant jet. In lowest order QCD, equivalent to the quark parton model, a single quark (antiquark) is scattered, leading to one current and one spectator jet — a (1+1) jet configuration. To next order in α_S, 2 jets are produced by gluon emission from the scattering quark (QCD Compton) and by the photon-gluon fusion process ($\gamma g \rightarrow q\bar{q}$) [1], leading to a (2+1) configuration. This makes for a more complex situation than in e^+e^- collisions where no strongly interacting particles are present in the initial state. Higher order QCD effects can be approximately described by parton showers as demonstrated in e^+e^- experiments. Exact QCD calculations to $\mathcal{O}(\alpha_S^2)$ have been performed for jet production in DIS [3] and so, with good event statistics, new precision tests of QCD are possible at HERA.

The H1 and ZEUS experiments have recently reported on first studies of global properties of hadronic final states in deep-inelastic scattering at HERA [4,5]. The ZEUS collaboration also presented results on the characteristics of jet production based on a cone algorithm [6]. In this letter we study the multi-jet production rates based on the JADE jet reconstruction algorithm [7], and compare the measurements with the predictions of QCD models. Preliminary results of the present analysis have already been presented [8].

2 Detector description

A detailed discussion of the H1 apparatus can be found elsewhere [9]. Here we describe briefly the components of the detector relevant to this analysis, which primarily makes use of the calorimeters, and to a lesser extent the central and backward tracking systems.

The scattered electrons and the hadronic energy flow are measured in a liquid argon (LAr) calorimeter and a lead-scintillator calorimeter (BEMC). Leaking hadronic showers are measured

---

[1] For presently accessible Q^2, Z^0 and $W^\pm$ exchange do not contribute significantly.

in a surrounding instrumented iron system. For the present analysis, the major part of the hadronic energy flow ($> 90\%$) is measured in the LAr calorimeter. The range $-3 < \eta < 3.2$ of pseudorapidity $\eta = -\ln(\tan\frac{\theta}{2})$ is used for the energy flow measurement. Here and elsewhere polar angles θ are defined with respect to the proton beam direction (z axis).

The liquid argon (LAr) calorimeter [10] extends over a polar angle range from $4^0 < \theta < 153^0$ with full azimuthal coverage. The calorimeter consists of an electromagnetic section with lead absorbers (EMC), corresponding to a depth between 20 and 30 radiation lengths, and a hadronic section with steel absorbers (HAC). The total depth of the LAr calorimeter varies between 4.5 and 8 hadronic interaction lengths. The calorimeter is highly segmented in both sections with a total of around 45000 geometric cells. The EMC (HAC) has a 3 to 4 (4 to 6) fold longitudinal segmentation. The lateral cell size in the forward region corresponds to about 1 Molière radius in the EMC and 1 interaction length in the HAC. The cells in the barrel region are approximately twice this size. The electronic noise per channel is typically between 10 and 30 MeV (1 σ equivalent energy). The method used to reconstruct the energy flow is described in [9,11].

Test beam measurements of the LAr calorimeter modules have demonstrated that the energy resolution is $\sigma_E/E \approx 12\%/\sqrt{E\ (\mathrm{GeV})}$ for electrons and $\approx 50\%/\sqrt{E\ (\mathrm{GeV})}$ for charged pions [9–11]. Both the hadronic energy scale and resolution from these beam tests have been verified from the balance of transverse momentum between hadronic jets and the scattered electron in DIS events, and they are known to a precision of 7% and 20% respectively. The uncertainty of the absolute scale for electrons is $\approx 3\%$.

The lead-scintillator calorimeter BEMC, with a thickness of 22 radiation lengths, covers the backward region of the detector ($151^\circ < \theta < 177^\circ$). The main task of the BEMC, besides the contribution to the energy flow measurement, is to trigger on and to measure electrons scattered from DIS processes with Q^2 values ranging from 5 to 100 GeV^2. The resolution is presently $10\%/\sqrt{E\ (\mathrm{GeV})} \oplus 3\%$. From a comparison of the measured electron energy in the BEMC with a determination using only the angles of both the hadronic system and the electron, the energy scale of the BEMC is known to 2%.

The calorimeters are surrounded by a superconducting solenoid providing a uniform magnetic field of 1.15 T along z in the tracking region. The return yoke surrounding this coil is fully instrumented with streamer tubes to measure leakage of hadronic showers and to recognize muons.

The main components of the tracking systems, which are located inside the calorimeters, are central drift and proportional chambers, a forward track detector, and a backward multiwire proportional chamber, covering the polar angle ranges $25^\circ < \theta < 155^\circ$, $7^\circ < \theta < 25^\circ$ and $155^\circ < \theta < 175^\circ$ respectively.

A scintillator hodoscope situated behind the BEMC is used to veto proton-induced background events based on their early time of arrival compared with nominal electron-proton collisions.

3 Data Selection

The analysis is split into a "low Q^2 sample" ($Q^2 < 80$ GeV^2) where the electron is measured in the BEMC, and a "high Q^2 sample" ($Q^2 > 100$ GeV^2) where the electron is measured in the LAr calorimeter. The systematic uncertainties and the event selection criteria are different for these samples. The hardware trigger for both samples is based only on the scattered electron so as to avoid any trigger bias in the hadronic final state.

Events in the "low Q^2 sample" satisfy the following requirements:

- an electron candidate in the BEMC, defined as a cluster associated with a space point in the backward proportional chamber, with angle $160^\circ < \theta_e < 172.5^\circ$ with respect to the proton beam axis,
- momentum transfer squared $Q^2 = 4E_eE_e' \cos^2(\theta_e/2)$ between 12 and 80 GeV^2, where E_e and E_e' are the energies of the incoming and scattered electron, and
- $E_e' > 14$ GeV, corresponding to $y \lesssim 0.5$, where the scaling variable $y = 1 - E_e'/E_e \sin^2(\theta_e/2)$, to eliminate possible background from photoproduction.

A more detailed discussion of triggering and event selection for this sub-sample can be found in [12].

The "high Q^2 sample" consists of events with the scattered electron detected in the LAr calorimeter. The electromagnetic cluster [9,11] in the LAr calorimeter with the largest transverse energy is considered as a candidate electron if it fulfills the following criteria:

- $Q^2 > 100$ GeV^2 and $y < 0.7$,
- it should be fully contained in the LAr calorimeter,
- it must not be associated (to within a cone of half opening angle of 5°) with a muon track candidate reconstructed in the instrumented iron (to reject cosmic showers),
- the energy deposited in the electromagnetic section in a cylinder of radius between 15 and 30 cm around the electron direction must be less than 1.2 GeV, and in the hadronic section within 30 cm around the electron direction must be less than 0.5 GeV ($\lesssim 1\%$ of clusters are lost by this isolation cut).

The following additional requirements are common to both samples:

- at least one charged particle track is demanded in the central tracking system to define an event vertex within ± 50 cm in z from the nominal interaction point, and
- $W^2 > 5000$ GeV^2, to ensure large enough hadronic energy flow into the detector. The invariant mass squared of the hadronic system, given by $W^2 = (p+q)^2$, with p and q the four-momenta of the incoming proton and virtual photon respectively, is evaluated using the angles of the electron and of the hadronic system (double angle method [13]).

The final low and high Q^2 samples contain 769 and 47 events respectively.

4 Jet Reconstruction

In the present analysis jets are reconstructed using the JADE algorithm [7] which was developed originally for e^+e^- interactions. The two main reasons for this choice are a) in Monte Carlo (MC) studies we find good correspondence between the jet rates calculated at the parton level and at the level of fully simulated and reconstructed events (see section 6), and b) higher order QCD predictions, to be compared with future larger data samples, are available on the basis of the JADE clustering scheme [3].

We reconstruct "particle" four-vectors using the energy in individual calorimeter cells and the vector joining the reconstructed event vertex with the centre of the cells. Use of clusters of calorimeter cells [9] as "particle" four-vectors instead of individual cells, yielded equivalent results. The invariant mass of all "particle" pairs (or combined objects) (i, j) is then calculated in the JADE algorithm using $m_{ij}^2 = 2E_iE_j(1 - cos\theta_{ij})$, thus neglecting the masses of "particles" i and j, and the pair with the smallest mass is taken to form a new combined object k by adding the four-vectors, $p_k = p_i + p_j$. The procedure is repeated until all remaining pairs have masses m_{ij} exceeding a cut-off which is defined by $m_{ij}^2 > y_{cut}M^2$, where y_{cut} is a resolution parameter and M is a mass scale taken to be the invariant mass of all objects entering the cluster algorithm ($\approx W$, including the beam pseudoparticle, see below). The energy deposition attributed to the scattered electron is excluded from this procedure. To account for the loss in the beam pipe of most hadrons from the proton remnant we introduce a pseudoparticle with a longitudinal momentum given by the missing longitudinal momentum of the event and no transverse momentum [14]. The final results given in section 6 are obtained with $y_{cut} = 0.02$, corresponding to a cut in m_{ij} of 10 to 30 GeV depending on W.

We investigated implementations of the JADE algorithm in alternative Lorentz frames and for different recombination schemes. We also tested other jet algorithms [15,16]. No significantly better agreement of the jet rates at the parton level with those obtained at the hadron level was achieved, both before and after full simulation of the detector.

5 QCD Models and Event Simulation

In QCD to $\mathcal{O}(\alpha_S)$ the 2+1 jet configuration is expected from the γ-gluon fusion process and the QCD Compton diagrams. Some of the models with which we will compare the data make explicit use of these matrix elements; others approximate the QCD effects with parton showers.

The model MEPS is based on the $\mathcal{O}(\alpha_S)$ matrix elements and an approximate treatment of higher order effects with leading-log parton showers. The model MEPS is implemented in the Monte Carlo generator LEPTO 6.1 [17]. We also use this generator without the parton showers (ME), and without parton showers and QCD matrix elements (QPM), to compare the data also with predictions from a simple quark parton model. Further we study in the frame of LEPTO a model (PSWQ) in which QCD effects are taken only to be leading-log parton showers with a scale $W \cdot \sqrt{Q^2}$. This scale fixes the maximum allowed virtuality at the beginning of the parton cascade. Extreme choices of scales such as W^2 and Q^2, are already excluded by previous data analyses [4,5]. In MEPS the scale for the parton showers is considerably restricted by the matrix element. The hadronization of partons follows the Lund string model as implemented in JETSET [18]. The PSWQ model includes QED radiation from the electron, which is achieved by combining the appropriate version of LEPTO with the radiative correction program HERACLES [19]. The radiative corrections for the (2+1) jet rates at $y_{cut} = 0.02$ are less then 5%.

In contrast with the Bremsstrahlung-like parton shower model used in LEPTO, the colour dipole model does not distinguish between initial and final state radiation and includes interference effects between them. It describes gluon emission by a chain of radiating colour dipoles, starting with a dipole formed between the scattered point-like quark and the extended proton remnant. We use the implementation of this model in ARIADNE [20], in which the scale is given by the p_t^2 of the radiated gluon with an upper limit proportional to $W^{4/3}$. Events are generated with LEPTO 6.1 for the electroweak interaction and for the γ-gluon fusion, followed by ARIADNE 4.03 which includes QCD Compton and further gluon emission in the framework of the colour dipole model. Such event simulations are henceforth referred to as CDM.

The data are also compared with the HERWIG event generator [21] where the QCD processes, without explicit $\mathcal{O}(\alpha_S)$ matrix elements, are based on leading-log parton showers which differ from those in LEPTO. Here the scale is essentially Q^2. It sets the upper limit for the shower evolution variables, which in HERWIG, in contrast to LEPTO, are related to energies and angles rather than to parton virtualities. As a result a more complete description of coherence effects is possible with HERWIG. For the final hadronization step, HERWIG uses a cluster fragmentation model.

No attempt has been made to tune the parameters of the models to the data in the new kinematical region at HERA. For LEPTO and ARIADNE the default parameters are used with the exceptions of $\Lambda_{QCD} = 200$ MeV and of the y_{cut} at the parton level (PARL(8)=0.0025 in case of MEPS and ME). For HERWIG we use a version specified by parameters suggested in [22]. None of the models, besides PSWQ (see above), contains radiative corrections.

The jet fractions predicted by the models depend also on the proton structure function used in the event generation. In particular the gluon distribution is important at low Q^2 due to the contribution of γ-gluon fusion to the jet production. In general we have assumed the MRSD0 parametrization [23]. The parton distributions in such a parametrization enter the prediction for the fraction of (2+1) jet events, R_{2+1}, in two ways. For the production of two non-remnant jets with $m_{ij}^2 > y_{cut} W^2$, the parton momentum fraction x of the proton which enters the hard scattering process must be larger than y_{cut} ($= 0.02$). For such parton x, present parton density parametrizations differ only marginally. On the other hand, the total number of events (in the denominator of R_{2+1}) averages over a Bjorken x range between 10^{-4} and 10^{-2} (for the low Q^2 sample) where the predictions of parton density parametrizations, based on extrapolations of fixed target data, are quite different. The predicted R_{2+1} at $y_{cut} = 0.02$ using the MRSD$^-$ parametrization [23], which is closer to the recent measurements of the proton structure function F_2 at HERA [12,24], is less than that using the MRSD0 parametrization by 0.025 in the lowest Q^2 bin of our event sample. At higher Q^2 this difference is smaller.

6 Results

In fig. 1 we show, for the low Q^2 sample and $y_{cut} = 0.02$, the flow of transverse energy, E_t, (transverse with respect to the beam) as a function of $\Delta\eta$ and $\Delta\phi$. Here $\Delta\eta$ and $\Delta\phi$ are the distance of the calorimeter cells from the jet axis in pseudorapidity η and azimuth ϕ (radians) for non-remnant jets found with the JADE algorithm. The angle ϕ is taken to increase away from the scattered electron for the jet at smallest η. The energy flow is shown for the (1+1) jet and the (2+1) jet events. For the (2+1) jet events, the profiles are shown separately for the jet at smaller (fig. 1c,d) and larger (fig. 1e,f) pseudorapidity η respectively. Also shown are the E_t flows actually attributed by the JADE algorithm to the jets. Distinct jet structures are observed for both event classes. The jets are predominantly at nearly opposite azimuth ϕ in the (2+1) jet event class (fig. 1c,e), as expected at low Q^2.

The simulations of the QCD models MEPS and CDM (the latter not shown in fig. 1) reproduce the gross features in shape and height of the observed $\Delta\eta$ and $\Delta\phi$ jet profiles. The same is true for the parton shower model PSWQ (not shown in fig. 1b) which, however, fails to describe the forward energy flow in the (1+1) jet events. For the (2+1) jet events the HERWIG model shows a lack of E_t flow in the region of the forward jet and between the jets (fig. 1d to f), and fails to describe the separation in ϕ (fig. 1c,e) [2].

The dependence of the jet rates on the resolution parameter y_{cut} (see section 4) is shown for the low and high Q^2 data sample in fig. 2a and b respectively. The data are not corrected for detector bias. R_{N+1} is the fraction of $(N+1)$ jet events in the sample. At $y_{cut} = 0.02$ the (1+1) and (2+1) classes dominate, with $R_{2+1} \approx 10$ to 20%. It should be noted that the data points in fig. 2 are strongly correlated as the same event sample is used for each value of y_{cut}. In this and the following figures only the statistical errors are given. Systematic effects are discussed in section 7.

To check if these rates can be taken as a measure of jet multiplicities at the parton level, the data in fig. 2a and b are compared to Monte Carlo predictions at the parton level (dotted curve), to the same model after hadronization (dashed curve), and to the prediction including a complete simulation of the H1 detector (full curve). In all cases the MEPS model is used. The figure demonstrates that in the high Q^2 sample hadronization and detector effects are small ($\approx$ 10%). For the low Q^2 sample the differences between these curves are larger ($\approx$ 15%) for $y_{cut} \gtrsim 0.02$. For lower values of y_{cut} more event structure is resolved as "jets" because the jet algorithm then fails to include individual hadrons in jet clusters.

It should be noted that the correspondence between parton and hadron jets is not "one to one" because there are migrations of events classified as (2+1) jet at the parton level to the (1+1) class at the hadron level and vice versa. This migration is because of the finite resolution of the y_{cut} value at which a (2+1) jet event is turned into a (1+1) event at the parton and hadron levels (see table 1).

All QCD-based models discussed in section 5 reproduce the main dependence on y_{cut} of the jet rates for both data samples, as shown in figs. 2c,d where the statistical errors due to the MC

---

[2] Neither of these discrepancies are affected using the available option of an "soft underlying event".

simulation are less than half those of the experimental data. The PSWQ model prediction of the (2+1) jet rate in the region around $y_{cut} = 0.02$ shows the most significant deviation from the data, namely by $\approx +50\%$ at $Q^2 < 80$ GeV^2. The fraction of (0+1) jet events (not shown in fig. 2), for which all the hadronic energy is attributed to the proton remnant jet, increases with y_{cut} somewhat more in the data than in the simulated models.

The Q^2 dependence of R_{2+1} (not corrected for detector bias) is shown in fig. 3 for fixed $y_{cut} = 0.02$ together with the expectation of the different models discussed above. The experimental points are well described by the MEPS model. R_{2+1} assuming the PSWQ model systematically exceeds the measurement. R_{2+1} using HERWIG and especially CDM shows little Q^2 dependence. R_{2+1} using the quark parton model (QPM, section 5, not shown in fig. 3) is $< 5\%$ of that measured.

The models with $\mathcal{O}(\alpha_S)$ matrix elements, especially MEPS, describe the observed energy flow and the jet fractions R_{N+1} in a satisfactory way without any further adjustment of parameters. We therefore correct the data in the above Q^2 bins for detector effects using the MEPS model and the simple ansatz

$$R^{corrected}_{(2+1)}(y_{cut} = 0.02, Q^2) = \frac{R^{MC\ hadrons}_{(2+1)}}{R^{MC\ recon.}_{(2+1)}} R^{data}_{(2+1)}(y_{cut} = 0.02, Q^2)$$

where $R^{MC\ hadrons}_{(2+1)}$ was obtained applying the JADE algorithm to the hadrons generated by MC, with $W^2 > 5000$ GeV^2, and for the low and the the high Q^2 sample $y < 0.5$. The fraction $R^{MC\ recon.}_{(2+1)}$ was obtained from MC events, subjected to a full simulation of the H1 detector and to the same analysis as the data. The corrections for detector effects do not exceed 20%. The corrected (2+1) jet rate is given in fig. 4 as a function of Q^2.

In the MEPS model, with present parameters, the $\mathcal{O}(\alpha_S)$ matrix elements dominate the contribution to R_{2+1}, but the addition of parton showers improves the description of the data. This can be seen in fig. 4 by comparing the predictions of MEPS with the model ME which contains the matrix elements but not the parton showers. The observed jet rate is mainly due to the γ-gluon fusion process. In the low (high) Q^2 sample $\approx 75\%$ ($\approx 50\%$) of (2+1) jet events simulated with MEPS are attributed to the γ-gluon fusion graph.

Because of the Q^2 dependence of the coupling constant α_S, the matrix element for jet production decreases with increasing Q^2. This decrease is not manifest directly in R_{2+1} because of the increase in phase space for jet production at higher Q^2, given the kinematic cuts of the present event sample and the jet definition. It is, however, interesting to test the sensitivity of the Q^2 variation of the (2+1) jet rate due to the running of α_S by comparing the data to a model with constant $\alpha_S = 0.25$ (fig. 4). The curve with a running coupling constant ($\Lambda = 200$ MeV) gives a slightly better description of the data. However the large statistical and systematic errors at this stage allow no quantitative discrimination.

7 Systematic Errors

The main sources of systematic uncertainty in the measured jet fractions are due to detector effects and the model dependent description of the hadronic final state. To quantify these contributions we use the variation of R_{2+1} at $y_{cut} = 0.02$.

The uncertainty of the energy calibration and resolution of the LAr calorimeter for this sample of low energy hadronic jets (7% and 20% respectively) leads to fractional errors of 7% and 10% for R_{2+1} respectively. The limited hadronic response of the BEMC calorimeter has little influence on R_{2+1}. Changing its calibration by 50% results in a fractional change of less than 5% for R_{2+1}.

Particles hitting material close to the beam in the forward region outside the detector acceptance can generate additional energy flow in the calorimeter. Increasing in simulation this additional energy flow by 50% leads to a fractional change for R_{2+1} of $\lesssim 5\%$. R_{2+1} obtained with both the JADE algorithm and the assumption of a pseudoparticle for the remnant jet is also quite insensitive to the calorimeter acceptance, despite the fact that in most cases one of the two non-remnant jets appears at small polar angle ($<\theta_{jet}>\approx 8^\circ$). For example a variation of the minimum polar angle near the beam pipe between 3.7 and 6.7° changes R_{2+1} for data and simulation (MEPS) by less than ±10%, and this is not included in the overall systematic error.

The corrections for detector bias of the jet fractions as a function of Q^2 are determined using the MEPS model and found to be less than 20%. A rough estimate of the model dependence is given by evaluating the corrections with different models, whence an estimate of the systematic uncertainty in using the MEPS model to correct for detector bias is 14%.

Adding the errors above in quadrature, we estimate a total systematic error of ±14% for the measured jet fraction in fig. 3, and an uncertainty of ±20% for the corrected jet fraction in fig. 4. These systematic errors will decrease with future larger data samples, where it will be possible to improve the calorimeter calibration and simulation and to tune the models.

8 Conclusion

Multi-jet production has been observed in the new kinematic domain of lepton scattering at HERA. The jets were reconstructed using the JADE algorithm, requiring jet-jet masses above 10 GeV or more (depending on W). Between 10 and 20% of the events contain 2+1 jets (2 high p_t and the proton remnant). Jet energy profiles and the dependence of multi-jet production rates on the jet resolution parameter and on Q^2 have been presented. It has been shown that hadronization and detector effects are small and controllable using the JADE jet reconstruction algorithm. A good overall description of multi-jet production is achieved using first order QCD matrix elements with higher order effects modelled by parton showers.

Acknowledgement We are grateful to the HERA machine group whose outstanding efforts made possible this experiment. We acknowlege the support of the DESY technical staff. We are grateful for the immense contributions of the engineers and technicians who constructed and who now maintain the H1 detector. We thank the funding agencies for financial support. We also wish to thank the DESY directorate for the hospitality extended to the non-DESY members of the collaboration.

References

[1] EMC, J.J. Aubert et al., Phys. Lett. B95 (1980) 306, Phys. Lett. B100 (1981) 433, Phys. Lett. B119 (1982) 233;
EMC, M. Arneodo et al., Z. Phys. C 36 (1987) 527;
E665 Collab., M.R. Adams et al. Phys. Lett. B272 (1991) 163.

[2] E665 Collab., M.R. Adams et al. Phys. Rev. Lett. 69 (1992) 1026, FERMILAB-Pub-93/171-E, submitted to Phys. Rev. Lett.

[3] D. Graudenz, Phys. Lett. B256 (1991) 518, preprint LBL-34147 (1993);
T. Brodkorb, J. G. Körner, Z. Phys. C54 (1992) 519. T. Brodkorb, J. G. Körner, E. Mirkes and G. A. Schuler Z. Phys. C44 (1989) 415;
F. A. Berends, W. T. Giele and H. Kuijf, Nucl. Phys. B321 (1989) 39;
K. Hagiwara and D. Zeppenfeld, Nucl. Phys. B313 (1989) 560.

[4] H1 Collab., T. Ahmed et al., Phys. Lett. B298 (1992) 469.

[5] ZEUS Collab., M. Derrick et al., Z. Phys. C59 (1993) 231.

[6] ZEUS Collab., M. Derrick et al., Phys. Lett. B306 (1993) 158.

[7] JADE Collab., W. Bartel et al., Z.Phys. C33 (1986) 23.

[8] M. Erdmann et al., *New Results from the H1 Experiment at HERA on Photoproduction, Deep Inelastic Scattering and Searches for New Particles*, DESY preprint 93-077 (1993);
A. De Roeck, *Deep Inelastic Scattering at Low-x. Results From the H1 Experiment*, DESY preprint 93-087 (1993).

[9] H1 Collab., I. Abt et al., *The H1 detector at HERA*, DESY preprint 93-103 (1993), to be submitted to Nucl. Instr. and Meth.

[10] H1 Calorimeter Group, B. Andrieu et al., *The H1 Liquid Argon Calorimeter System*, DESY preprint 93-078 (1993), to be published in Nucl. Instr. and Meth.

[11] H1 Calorimeter Group, B. Andrieu et al., DESY preprint 93-047 (1993), *Results from Pion Calibration Runs for the H1 Liquid Argon Calorimeter and Comparisons with Simulations*, to be published in Nucl. Instr. and Meth.

[12] H1 Collab., I. Abt et al., DESY preprint 93-117 (1993), Nucl. Phys. B407 (1993) 515.

[13] S. Bentvelsen et al. Physics at HERA, Proceedings of the workshop, Eds. W. Buchmüller, G. Ingelman Hamburg (1991), Vol. 1, 23.
K. C. Hoeger, ibid., Vol. 1, 43.

[14] D. Graudenz, N. Magnussen, Physics at HERA, Proceedings of the workshop, Eds. W. Buchmüller, G. Ingelman Hamburg (1991), Vol. 1, 261;
M. Fleischer et al., ibid., Vol. 1, 303;
M. Crombie and A. Wegner, ibid., Vol. 1, 321.

[15] S. Catani et al., Phys. Lett. B269 (1991) 432; S. Catani et al., Phys. Lett. B285 (1992) 291.

[16] L. Lönnblad, *A new jet clustering algorithm inspired by the colour dipole model*, DESY preprint 92-181 (1992).

[17] G. Ingelman, “LEPTO 6.1”, Physics at HERA, Proceedings of the workshop, Eds. W. Buchmüller and G. Ingelman, Hamburg (1991) Vol. 3, 1366, and references therein.

[18] T. Sjöstrand, Comp. Phys. Commun. 39 (1986) 347;
T. Sjöstrand and M. Bengtsson, Comp. Phys. Commun. 43 (1987) 367, and for JETSET 7.3,
T. Sjöstrand, CERN-TH-6488-92 (1992).

[19] A. Kwiatkowski, H. Spiesberger, and H.-J. Möhring, Comp. Phys. Commun. 69 (1992) 155, and references therein.

[20] L. Lönnblad, Comp. Phys. Commun. 71 (1992) 15, and references therein.

[21] G. Marchesini et al. Comput. Phys. Commun. 67 (1992) 465 and references therein.

[22] N. Magnussen et al., Physics at HERA, Proceedings of the workshop, Eds. W. Buchmüller, G. Ingelman Hamburg (1991), Vol. 3, 1167.

[23] A.D.Martin, W. J. Stirling and R. G. Roberts, Phys. Rev. D47 (1993) 867.

[24] ZEUS Collab., M. Derrick et al., DESY preprint 93-110 (1993).

		low Q^2 sample		high Q^2 sample	
a)		detector level			
	jet classes	not (2+1)	(2+1)	not (2+1)	(2+1)
hadron level	not (2+1)	0.86	0.05	0.75	0.07
	(2+1)	0.04	0.05	0.06	0.12
b)		hadron level			
	jet classes	not (2+1)	(2+1)	not (2+1)	(2+1)
parton level	not (2+1)	0.88	0.03	0.74	0.07
	(2+1)	0.03	0.06	0.08	0.11

Table 1: *Probabilities for the events in the two Q^2 samples to be classified as (2+1) jet or other (predominantly 1+1) at $y_{cut} = 0.02$. The MEPS simulation has been used to correlate the multiplicities a) at the hadron and detector level, and b) at the parton and hadron level.*

Figure 1:
Transverse energy flow for the low Q^2 sample as a function of $\Delta\phi$ and $\Delta\eta$, each with respect to the jet axis of non-remnant jets, for (1+1) jet events (a,b respectively) and for (2+1) jet events (c,d and e,f for the jets with smaller and larger η respectively). The sense of ϕ is away from the scattered electron for the jet at smallest η. The points ($\bullet$) are the data, and the dashed and dotted lines show the E_t flow attributed by the JADE algorithm to the jet at smaller or larger η respectively. The open and shaded histograms are Monte Carlo simulations using MEPS and HERWIG respectively.

Figure 2:
Fractions of N+1 jets (R_{N+1}) versus the cut variable of the jet algorithm for $12 < Q^2 < 80$ GeV^2 (a,c) and $Q^2 > 100$ GeV^2 (b,d), compared in a),b) with simulation with MEPS at the detector level, at the hadron level and at the parton level, and in c),d) to predictions from the QCD based models MEPS, CDM, PSWQ and HERWIG.

Figure 3:
Uncorrected (2+1) jet fraction R_{2+1} at $y_{cut} = 0.02$ versus Q^2 compared with different QCD based models: MEPS, CDM, PSWQ and HERWIG. The vertical error bars correspond to the statistical errors. For systematic errors see section 7.

Figure 4:
(2+1) jet fraction R_{2+1} at $y_{cut} = 0.02$ versus Q^2, corrected for detector bias for $W^2 > 5000$ GeV^2 and $y < 0.5$, in comparison with the MEPS model with a running α_S and a constant $\alpha_S = 0.25$, and also with the matrix elements but no parton showers (ME model). The data are plotted at the corrected $< Q^2 >$ per bin. The error bars correspond to the statistical errors of data and MC correction. For systematic errors see section 7.

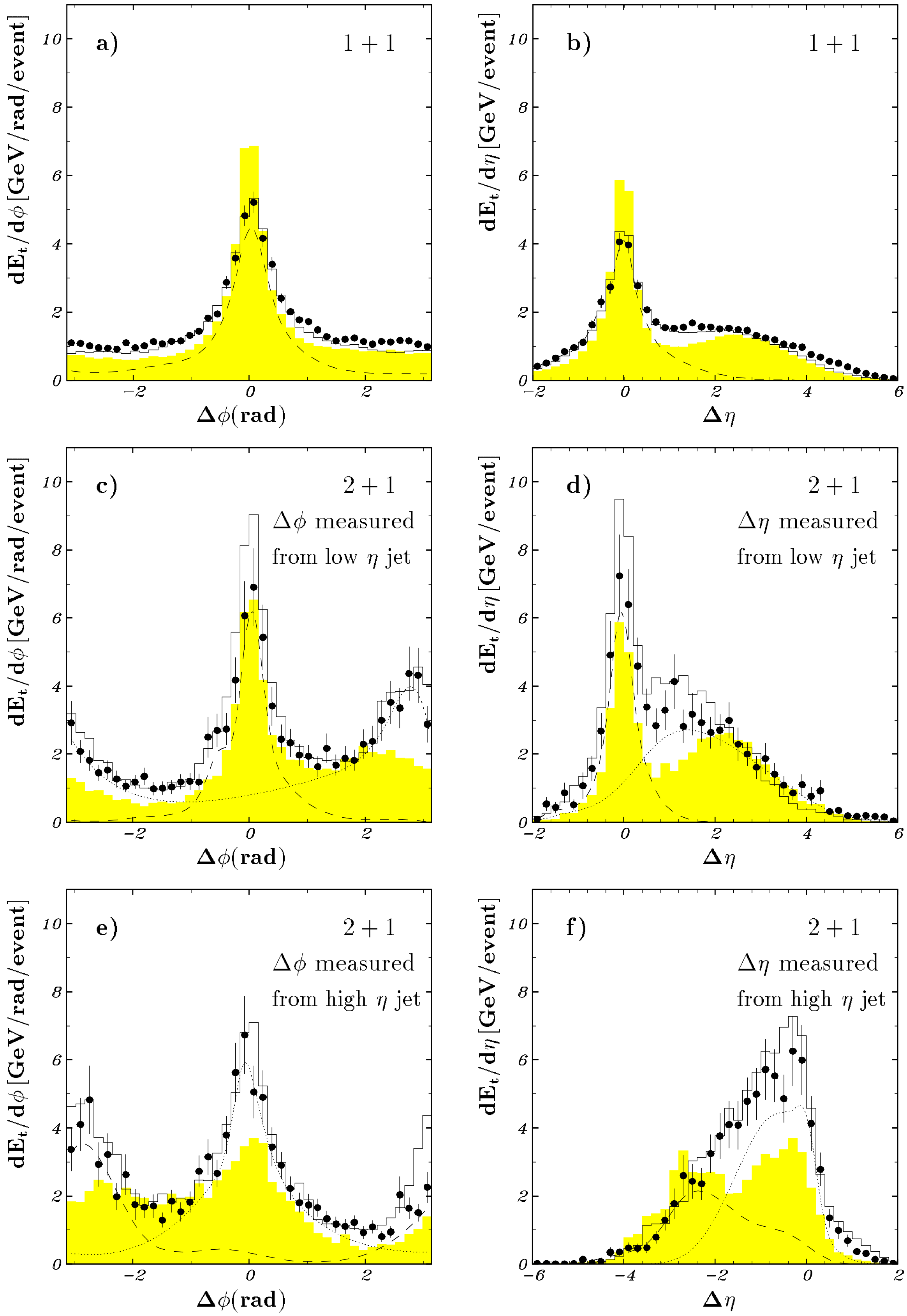
a)
1 + 1
b)
1 + 1
c)
2 + 1
$\Delta\phi$ measured
from low η jet
d)
2 + 1
$\Delta\eta$ measured
from low η jet
e)
2 + 1
$\Delta\phi$ measured
from high η jet
f)
2 + 1
$\Delta\eta$ measured
from high η jet
$dE_t/d\phi$ [GeV/rad/event]
$dE_t/d\eta$ [GeV/event]
$\Delta\phi$(rad)
$\Delta\eta$
0
2
4
6
8
10
−2
0
2
−2
0
2
4
6
−6
−4
−2
0
2

Figure 1

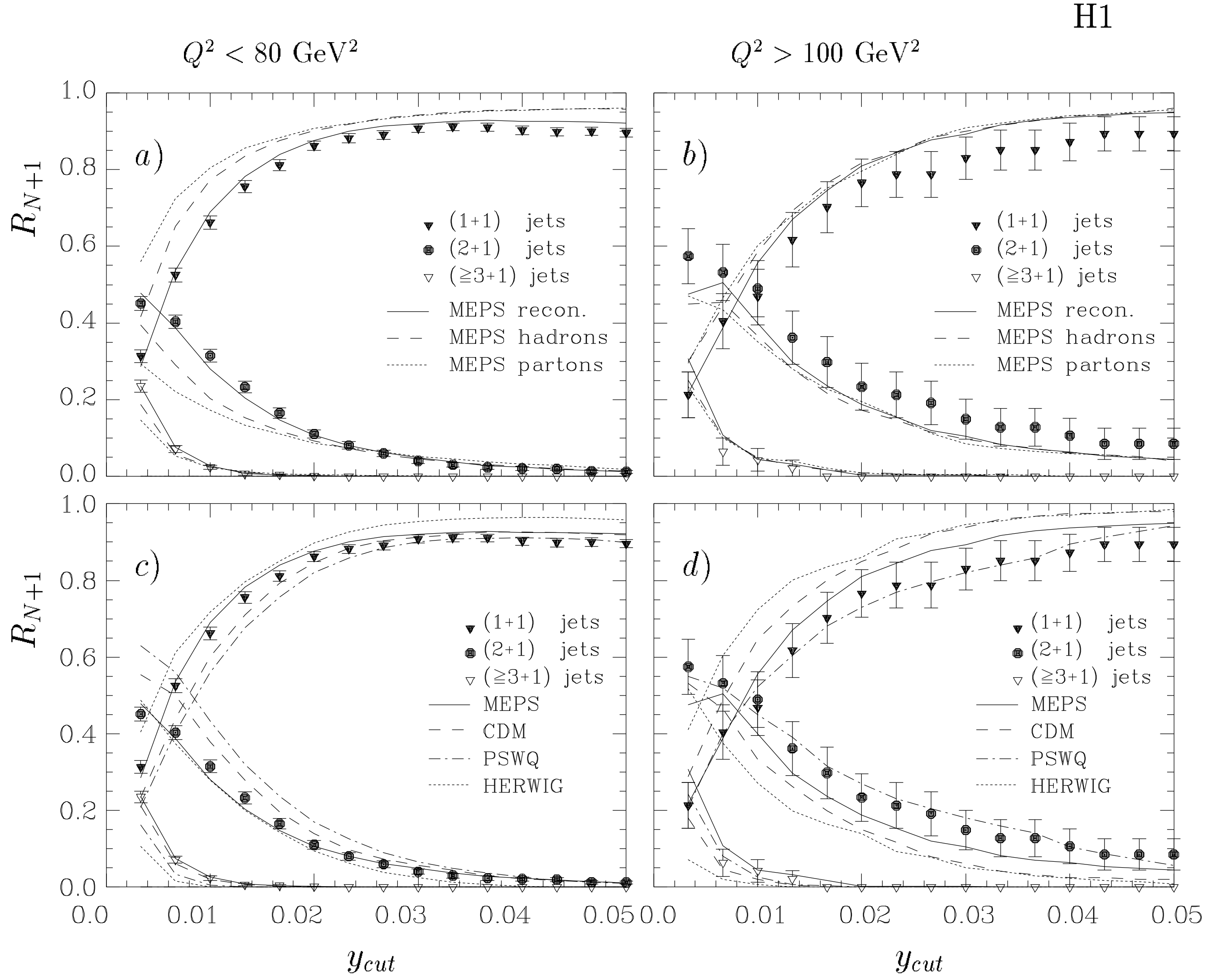
H1
$Q^2 < 80$ GeV^2
$Q^2 > 100$ GeV^2
R_{N+1}
a)
b)
c)
d)
(1+1) jets
(2+1) jets
(≥3+1) jets
MEPS recon.
MEPS hadrons
MEPS partons
MEPS
CDM
PSWQ
HERWIG
0.0
0.2
0.4
0.6
0.8
1.0
0.01
0.02
0.03
0.04
0.05
y_{cut}

Figure 2

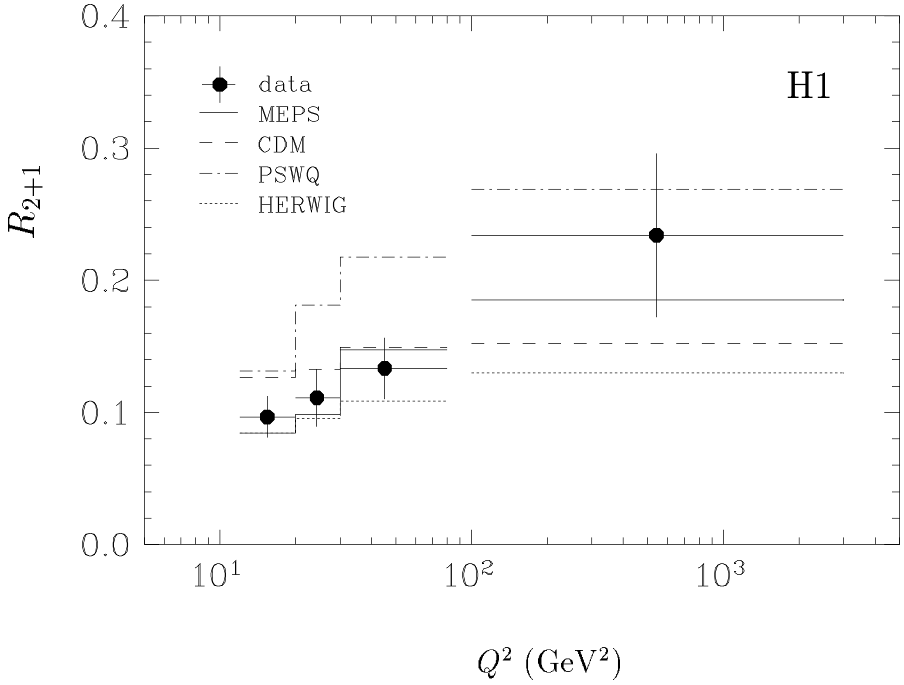

Figure 3

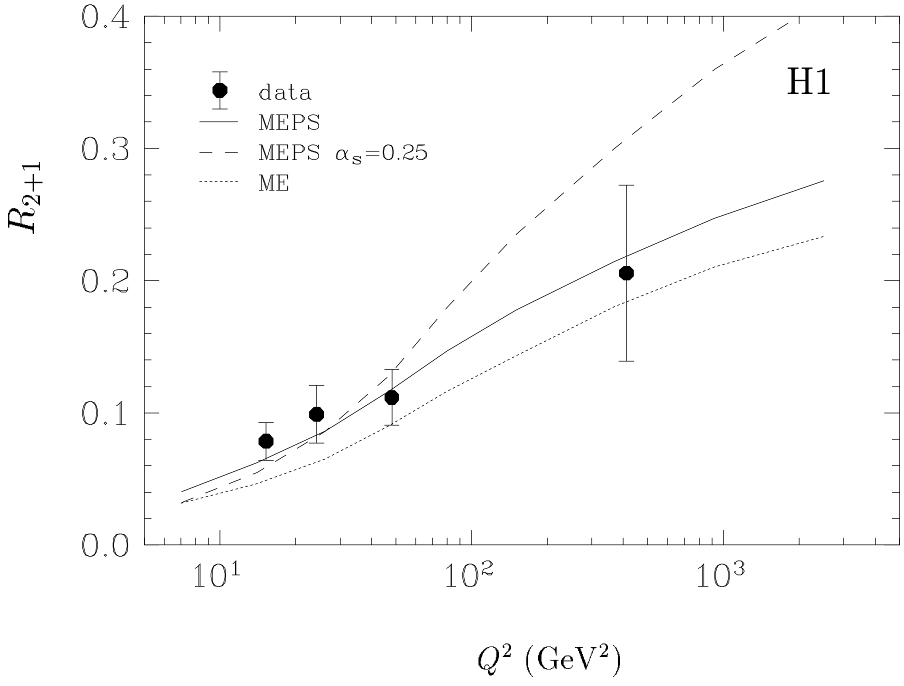

Figure 4